

Matrix Stiffness Induces Midnolin-dependent Lamin B1 Degradation to Control Myoblast Differentiation

Liping Guo^{1,2,8}, Yanjing Zhao^{2,3,8}, Zhe Zhang², Chang Sun^{2,4}, Yafan Xie⁵, Qin Dai^{6,7}, Yan Yan³, Yaoqi Zhou², Yang Zhang², Quhuan Li^{1,*}, Juhui Qiu^{5,*}, Qin Peng^{2,*}

¹ School of Biology and Biological Engineering, South China University of Technology, Guangzhou, China.

² Shenzhen Bay Laboratory, Shenzhen, China.

³ Division of Life Science, Hong Kong University of Science and Technology, Clear Water Bay, Kowloon, Hong Kong, China.

⁴ Department of Pathology and Experimental Therapeutics, Faculty of Medicine and Health Sciences, Barcelona University, Barcelona, Spain.

⁵ Key Laboratory for Biorheological Science and Technology of Ministry of Education, State and Local Joint Engineering Laboratory for Vascular Implants, College of Bioengineering, Chongqing University, Chongqing, China.

⁶ Shenzhen Medical Academy of Research and Translation (SMART), Shenzhen, Guangdong, China

⁷ Westlake University, Hangzhou, China

⁸ These authors contributed equally.

*Correspondence: pengqin@szbl.ac.cn (Q.P.), jhquiu@cqu.edu.cn (J.Q.), liqh@scut.edu.cn (Q.L.)

Abstract

Cells decode mechanical cues to direct fate decisions through nuclear remodeling, yet nuclear adaptors to mechanical signals remain elusive. Here, we show that soft matrix suppresses myoblast differentiation and induces nuclear abnormality within 30 minutes, accompanied by a >60% reduction in lamin B1 proteins levels. Mechanistically, midnolin interacts with lamin B1 and mediates ubiquitination-independent degradation of lamin B1 on soft matrix, through the Catch domain of midnolin engaging a β -strand within lamin B1's Ig-like domain. Functionally, moderate lamin B1 expression is essential for myoblast differentiation initiation, as its depletion either by siRNA or CRISPR knockout abolishes myogenic capacity. Our findings reveal that the midnolin-proteasome axis directly converts mechanical inputs into lineage commitment by triggering lamin B1 degradation, defining a novel nuclear mechano-adaptation pathway.

Keywords: Matrix stiffness; Lamin B1 degradation; midnolin-proteasome pathway; myoblast differentiation

The final character: 26,241

1 Introduction

2 Mechanical stimuli in the cellular microenvironment are powerful regulators of cell function
3 and behavior, such as extracellular matrix (ECM) elasticity and mechanical strain can
4 significantly influence the fate decision of stem and progenitor cells (Baghdadi *et al*, 2024;
5 Shiraishi *et al*, 2023). The basic mechanism is that stem cells sense mechanical cues and then
6 active downstream signaling events and ultimately results in cell fate transitions and even
7 participates in diseases development (Fiore *et al*, 2025). For example, studies in satellite cells
8 or the differentiation of muscle progenitor cells (Kjaer, 2004; Thomas *et al*, 2015; Zhang *et al*,
9 2021) revealed that the structural remodeling and stiffness of the extracellular matrix are
10 involved in Duchenne muscular dystrophy (Long *et al*, 2024), both reduced mechanical loading
11 and low ECM stiffness suppress cell differentiation and muscle regeneration, causing muscle
12 disuse atrophy (Gibbons *et al*, 2018; Kjaer, 2004; Wall *et al*, 2013). Hence, the cellular and
13 molecular mechanistic understanding of how cells sense mechanical cues are still the potential
14 mechanical determinators of cell fate.

15 The nucleus, as the stiffest cellular organelle, perceives mechanical cues through cytoskeletal
16 connections and the linker of nucleoskeleton and cytoskeleton (LINC) complex-mediated
17 mechanotransduction (De Belly *et al*, 2022; Dupont & Wickstrom, 2022; Kalukula *et al*, 2022;
18 Maurer & Lammerding, 2019; Nava *et al*, 2020). This mechanosensing capability enables
19 dynamic modulation of nuclear morphology and transcriptional programs, ultimately
20 influencing cell fate decisions. On stiff matrices, nuclei typically adopt a flattened and
21 elongated morphology, which is associated with differentiated cell states. In contrast, on soft
22 matrices, nuclei remain more rounded, exhibiting nuclear envelope (NE) wrinkling and reduced
23 volume-a configuration that helps maintain stem cell pluripotency (Cosgrove *et al*, 2021; Lovett
24 *et al*, 2013; Nguyen *et al*, 2024; Price *et al*, 2017; Virdi & Pethe, 2022). The proper adaptation
25 from the nucleus to the extracellular mechanics is typically called nuclear mechano-adaptation,
26 which requires the nuclear skeleton to rapidly adapt the changes to maintain nuclear integrity
27 (Echarri *et al*, 2019). However, there are lacking a precise explanation of the temporal and
28 molecular basis underpinning nuclear adaptation to the mechano-microenvironment (Beedle &
29 Roca-Cusachs, 2023).

30 NE proteins maintain the structural integrity and stability of the nuclei. Loss of nuclear skeleton
31 lamina proteins can cause nuclear envelope wrinkling and alterations in nuclear volume
32 (Vahabikashi *et al*, 2022). Previous studies showed that loss of lamin A tends to increase
33 nuclear volume while loss of lamin B1 behaves in the opposite way (Swift *et al*, 2013;
34 Vahabikashi *et al*, 2022). Lamin B1 expression is responsible for nuclear elasticity to stabilize
35 chromatin condensation (Wintner *et al*, 2020). However, the timescales and mechanism on how
36 lamin B1 loss adapts to the mechano-microenvironment is not well understood. Currently, there

are three pathways related to protein loss or degradation, which are ubiquitination-dependent proteasome pathway (Pohl & Dikic, 2019), midnolin-proteasome pathway for ubiquitination-independent degradation (Gu *et al*, 2023), as well as autophagy-lysosomal pathway (Pohl & Dikic, 2019). It is reported that lamin B1 undergoes degradation through ubiquitination-regulated pathways by E3 ligases (Khanna *et al*, 2018; Krishnamoorthy *et al*, 2018), or autophagic degradation after oncogenic damage (Dou *et al*, 2015). The mechanism underlying ECM stiffness-dependent regulation of lamin B1 proteostasis remains unclear.

In this study, we observed the significant reduction of myoblast differentiation on soft matrices, which was attributed to time-dependent nuclear abnormalities. We analyzed that the major change of nuclear membrane proteins was lamin B1 reduction on soft matrix. To elucidate the underlying mechanism, we investigated different pathways that regulate proteostasis and identified that midnolin mediated lamin B1 degradation via a β -strand capture mechanism in the ubiquitination-independent proteasome pathway on soft matrix. Furthermore, we explored the consequences of lamin B1 reduction in myoblast differentiation. We found that lamin B1 upregulation is required in the early stages of differentiation and influences key myoblast differentiation regulators: *Myod1* and *Wnt4*. Our findings suggest that lamin B1 serves as a critical regulator of nuclear mechanoadaptation and is indispensable for proper myoblast differentiation.

Results

Soft Matrix attenuates myoblast differentiation related to nuclear abnormalities

To explore the effect of mechanical cues on muscle cell differentiation, mouse myoblasts were cultured on fibronectin (FN)-coated polyacrylamide (PAA) hydrogels with stiffnesses of 0.2 kPa (soft), mimicking atrophic muscle conditions, and 10 kPa (stiff), resembling healthy muscle stiffness (Fig. 1A and EV1A). RNA sequencing (RNA-seq) categorized the biological process of differentially expressed genes (DEGs) by Gene Ontology (GO) analysis, revealing significant alternations in cell fate and differentiation catalogers under soft matrix condition (Fig. 1B).

We further induced primary myoblast differentiation with 2% horse serum on different stiffness matrix. Our results demonstrated that myoblast fusion, as indicated by myosin heavy chain 4 (MYH4) expression, was markedly suppressed on soft matrices relative to stiff matrix following 7 days of differentiation induction (Fig. 1C-E). Similar results were from myoblast cell line C2C12 after 7 days induction (Fig. 1F-H), and this inhibition was evident as early as day 3 (Fig. EV1B, C).

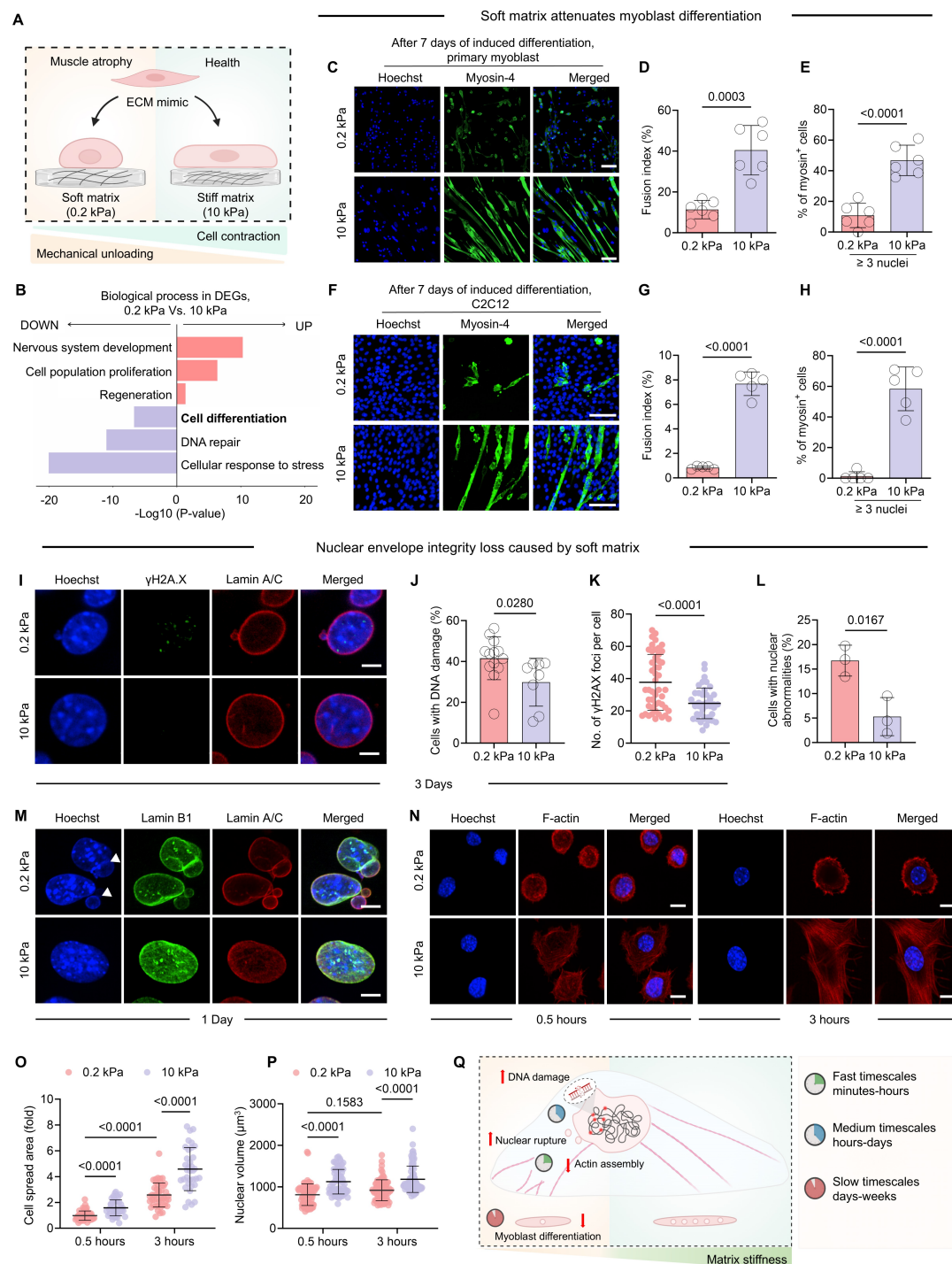


Figure 1. Soft matrix impairs myoblast differentiation and increases nuclear abnormalities and DNA damage.

(A) Schematic of hydro-matrices with different stiffness to mimic mechanical loading on cells in healthy and muscular dystrophy conditions (figure created with BioRender.com). (B) GO terms analysis of biological processes for upregulated and downregulated genes (0.2 kPa Vs. 10 kPa) after 12 hours culturing on matrices. (C to H) Representative images of differentiated mouse primary myoblast cells (C) and C2C12 cells (F) on 0.2 kPa and 10 kPa matrices after 7 days of 2% horse serum induction. scale bar, 100 μm. (D, E, G, H) Quantification data of the fusion index and the percentage of myosin⁺ cells that ≥ 3 nuclei in (C) and (F), respectively. N = 7 (D and E), 5 (G and H). (I to K) Representative images from C2C12 cells seeded on 0.2 kPa and 10 kPa matrices after 3 days of horse serum induction. Hoechst for nuclear staining in blue, γH2AX staining in green and lamin A/C staining in red. Scale bars, 5 μm.

(J, K) The Quantification of cell numbers with DNA damage (J) and γ H2AX foci (K) in (I). $n > 40$ cells for each condition. **(L)** Quantification of cells with nuclear abnormalities in (M). **(M)** Representative images from C2C12 cells seeded on 0.2 kPa and 10 kPa matrices after 1 days of horse serum induction. Hoechst for nuclear staining in blue, lamin B1 staining in green and lamin A/C staining in red. Scale bars, 5 μ m. $n = 3$. **(N to P)** Immunofluorescence of C2C12 cells seeded onto 0.2 kPa and 10 kPa at 0.5 hours and 3 hours, respectively. Hoechst for nuclear staining in blue and F-actin staining in red. Scale bars, 10 μ m. Fold changes of cell spread area (O) and nuclear volume (P) were quantified from (N). $n > 50$ cells for each group. Data are presented as the mean \pm SD. Tukey's multiple comparisons test. **(Q)** Summary of hypothesis for soft matrix - mediated inhibition of myoblast differentiation (figure created with BioRender.com). Data information: data in (D, E, G, H, J, K and L) were presented as the mean \pm SD. Two-tailed Student's *t*-test was used for statistical analysis.

RNA-seq also indicated the enrichment of the pathway related to DNA repair (Fig. 1B), suggesting that the impaired myoblast differentiation might be associated with the accumulation of DNA damage. To test this hypothesis, we checked DNA damage dynamics in cells cultured on matrix of varying stiffness during the initial 72-hour differentiation period. More phosphorylated H2AX at Ser139 (γ H2AX)-positive nuclei were detected on soft matrix (Fig. 1I-K), demonstrating that soft matrix caused more DNA damage and may subsequently affected myoblast differentiation. Furthermore, nuclear abnormalities formed prior to a bulk accumulation of γ H2AX. Immunostaining revealed a significant alteration of nuclear morphology in 1 Day (Fig. 1M). In particular, 16.7% C2C12 cells cultured on soft matrix displayed a marked increase in nuclear blebbing and micronuclei (MN) formation (Fig. 1L). In addition, immunostaining results showed that soft matrix hindered F-actin assembly in the early stage of cell adhesion (0.5 hours) followed by gradual spreading (3 hours) in C2C12 (Fig. 1N, O). Nucleus, as a mechanosensor, responds to external forces transmitted from the cytoskeleton and deforms accordingly (Kalukula *et al.*, 2022). Our results showed a significant reduction in nuclear volume on soft matrix, compared to stiff matrices (Fig. 1P). Taken together, myoblast differentiation is inhibited when myoblasts cultured on soft matrix. Our findings indicate that this inhibition involves a time-dependent cellular adaptation process. Initially, within several minutes, cells on soft matrix exhibited reduced spreading capacity and nuclear volume. Subsequently, within several hours, nuclear morphological abnormalities emerged, subsequently triggering γ H2AX foci formation as a marker of DNA damage response. These sequential events collectively contribute to the suppression of myoblast differentiation over extended culture periods (Fig. 1Q).

Lamin B1 Decreases with Reduced Nuclear Volume on Soft Matrix

Nucleus abnormalities are influenced by NE proteins such as lamin A/C and lamin B1, which serve as nuclear skeleton with mechanical properties (Vahabikashi *et al.*, 2022). Therefore, we were curious about how nuclear envelop proteins are responsible for maintaining nucleus morphology and volume on matrix. Here we screened the level changes of the majority of NE proteins that have been reported to be associated with mechano-signaling pathways (Donnalaja

1 *et al.*, 2019; Kalukula *et al.*, 2022) by western blot, including Nucleoporin 153 (NUP153),
2 SUN1/2, lamin B receptor (LBR), emerin, lamina associated protein 2 (LAP2), lamin A/C,
3 lamin B1 (Fig. 2A). Our western blot results showed that the protein levels of lamin A/C was
4 lower on soft matrix as previously reported (Swift *et al.*, 2013), meanwhile both lamin B1 and
5 LAP2 decreased significantly on soft matrix (Fig. 2B). Based on the quantitative analysis,
6 reduction of lamin B1 protein level on soft matrix was the most among all the NE proteins at
7 0.5 hours post cell seeding (Fig. 2B, C). Additionally, lamin B1, which is critical for myoblast
8 differentiation, represents a novel mechanism in nuclear mechano-adaptation. Therefore, we
9 selected lamin B1 as a biomarker to investigate nuclear mechanosensing dysregulation in
10 muscle atrophy. Immunostaining further confirmed that lamin B1 protein level reduced on soft
11 matrix (Fig. 2D, E). This reduction was similarly observed in primary myoblasts (Fig. 2F, G),
12 confirming the substrate-dependent regulation of lamin B1. Next, we detected lamin B1 protein
13 levels over a day and found that the low lamin B1 level on soft matrices was retained over the
14 time from 0.5 hours to 24 hours (Fig. 2H, I). Altogether, these results implicate that matrix
15 stiffness modulates the physical deformation of nucleus via modulation of lamin B1 protein
16 level.

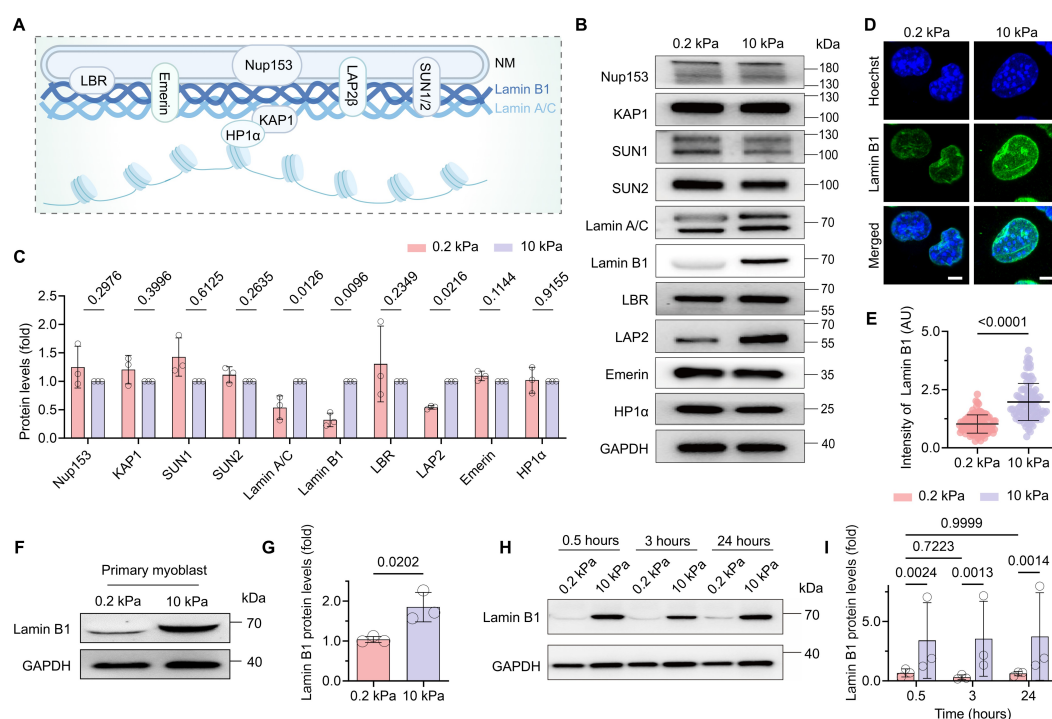


Figure 2. Soft matrix induces a significant reduction in lamin B1 and maintains this difference over the time consistently.

(A) Schematic diagram of some NE proteins (figure created with BioRender.com). (B, C) Western blot analysis of NE proteins displayed in (A) from C2C12 seeding onto PAA matrices after 0.5 hours. n = 3, Data are presented as the mean ± SD. Two-tailed Student's *t*-test. (D) Immunofluorescence of C2C12 cells on 0.2 kPa and 10 kPa substrates. Hoechst for nuclear staining in blue and lamin B1 staining in green. Scale bars, 4 μm. (E) Quantitative analysis of fluorescence intensity of lamin B1 on 0.2 kPa and 10 kPa substrates from (D) (> 300 cells for each group, Two-tailed Student's *t*-test, Data are presented as the mean ± SD). The fluorescence intensity unit is arbitrary (AU) and is defined from the detected total

fluorescence intensity normalized. **(F, G)** Western blot analysis of lamin B1 proteins in mouse primary myoblast cells seeded onto 0.2 kPa and 10 kPa matrices after 0.5 hours. $n = 3$. Two-tailed Student's *t*-test, Data are presented as the mean \pm SD. **(H, I)** Western blot analysis of lamin B1 proteins in C2C12 cells seeded onto matrices at different times. $n = 3$, Two-way ANOVA/Tukey's multiple comparisons test, Data are presented as the mean \pm SD.

Lamin B1 is Degraded by Proteosome Pathway on Soft Matrix

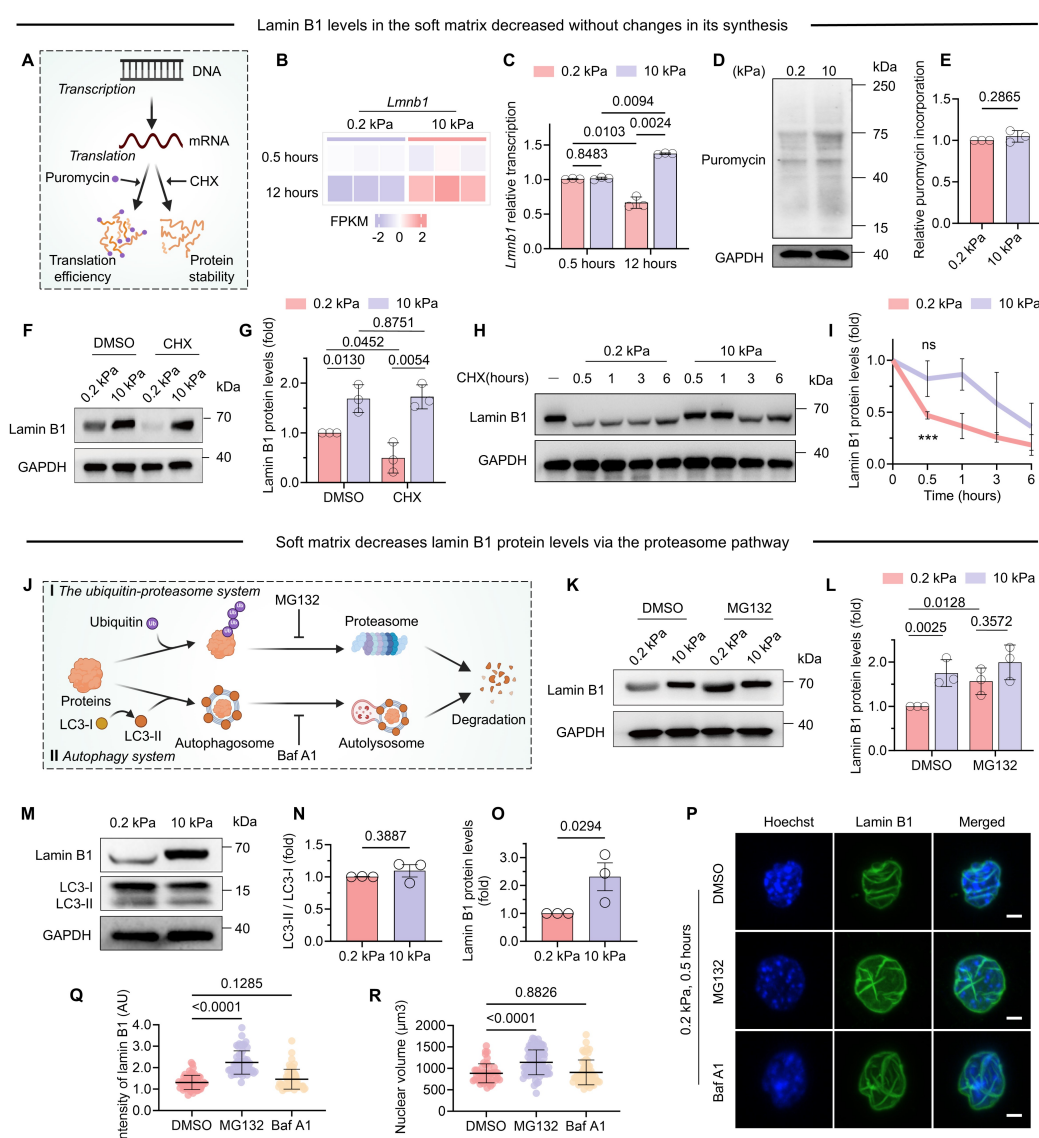
Cells maintain proteostasis by dynamically balancing protein synthesis and degradation in response to external stimuli. To elucidate the mechanism underlying the differential lamin B1 expression observed between 0.2 kPa and 10 kPa matrix, we investigated whether this regulation was mediated through changes in protein synthesis or altered degradation kinetics (Fig. 3A).

To investigate the influence of matrix stiffness on lamin B1 protein synthesis, firstly we performed RNA sequencing analysis of C2C12 myoblasts cultured on matrix of varying stiffness at two critical timepoints (0.5 hours and 12 hours) post-seeding. RNA-seq analysis demonstrated comparable mRNA expression levels of *Lmnbl* between soft and stiff matrix at 0.5 hours. However, by 12 hours, stiff matrices exhibited significantly elevated *Lmnbl* transcript levels. These findings indicate that the rapid decline in lamin B1 protein observed on soft matrix (Fig. 2B) is mediated through post-transcriptional regulation rather than reduced gene expression (Fig. 3B, C). Secondly, to determine whether translation was mediated by matrix stiffness, we confirmed by puromycin incorporation that global protein synthesis is unaffected by substrate stiffness (Fig. 3D, E). C2C12 myoblasts were then plated onto soft or stiff matrices in the presence or absence of cycloheximide (CHX), a selective inhibitor of translational elongation (Fig. 3A). CHX was added to the cell suspension before seeding. Our results showed that, lamin B1 protein level decreased significantly on soft matrix after 0.5 hours of CHX treatment compared to DMSO group (Fig. 3F, G), whereas no change was observed on stiff matrix, suggesting that matrix stiffness does not affect protein translation in adhesion process.

To measure the kinetics of lamin B1 protein degradation when cells were exposed to soft and stiff matrix, we treated C2C12 cells with CHX at different time points to assess the stability of lamin B1. Our results showed that B1 exhibited degradation kinetics on 0.2 kPa matrix, with significant protein loss detectable within 30 minutes of treatment. In contrast, lamin B1 remained stable for at least 60 minutes on 10 kPa matrix (Fig. 3H, I), demonstrating stiffness-dependent regulation of lamin B1 proteostasis.

Collectively, our findings demonstrate that accelerated protein degradation serves as the primary mechanism underlying the depletion of lamin B1 on soft matrix. Protein degradation occurs primarily through two evolutionarily conserved pathways: the ubiquitin-proteasome system and autophagy-lysosome pathway, which collectively mediate the controlled breakdown of proteins into reusable amino acids and short peptides (Fig. 3J) (Balchin *et al*, 2016; Pohl &

1 Dikic, 2019). Inhibition of proteasomal degradation using MG132 attenuated the decrease in
2 lamin B1 protein level on soft matrix, while there was no effect on the cells on stiff matrix (Fig.
3 3K, L). A similar trend was observed upon treatment with bafilomycin A1 (Baf A1), which
4 blocks autophagosome–lysosome fusion, suggesting that multiple degradation pathways may
5 be involved under soft matrix (Fig EV2A, B). To examine potential autophagic degradation, we
6 monitored LC3 lipidation, a marker of autophagy pathway activation (Fig. 3J). Quantitative
7 analysis revealed no significant difference in the LC3-II/LC3-I ratio between soft and stiff
8 matrix (Fig. 3M-O). Immunofluorescence results further confirmed lamin B1 protein level and
9 nuclear volume was significantly recovered with MG132 treatment but not Baf A1 (Fig. 3P-R).
10 These results demonstrate the proteasome-dominant degradation of lamin B1 protein is
11 regulated by matrix stiffness.



12

13 **Figure 3. Lamin B1 degradation on soft matrix through proteasome pathway.**
14 (A) Schematic diagram of classical protein synthesis pathway. Puromycin is incorporated into nascent

polypeptides to detect protein synthesis and assess translation efficiency. Cycloheximide (CHX) inhibits ribosomal activity to block new protein synthesis, enabling tracking of pre-existing protein decay for stability analysis. (Created with BioRender.com). **(B)** Representative genes from RNA-seq were upregulated in pink and downregulated in violet after 0.5 hours and 12 hours culturing on gels (0.2 kPa Vs. 10 kPa). **(C)** The expression of *Lmnbl* from RNA-seq after 0.5 hours and 12 hours culturing on gels (0.2 kPa Vs. 10 kPa). **(D, E)** C2C12 were treated with 91 μ M puromycin for 5 min after seeding onto gels for 25 min and immunoblotted for puromycin. $n = 3$. **(F, G)** Western blot analysis of lamin B1 protein in C2C12 seeded onto 0.2 kPa and 10 kPa gels for 0.5 hours in the presence of protein synthesis inhibitor (CHX, 50 mg/mL). $n = 3$. **(H, I)** Western blot analysis of lamin B1 proteins stability in C2C12 before seeding (-) and post-seeding onto 0.2 kPa and 10 kPa gels under cycloheximide (CHX) treatment to inhibit protein translation. $n = 3$. At 0.5 hour, compared to the condition before seeding ($t=0$), lamin B1 protein level showed a significant decrease on 0.2 kPa gel (***, $p < 0.001$), while no significant change was observed on 10 kPa gel (ns, no significance). Data are presented as the mean \pm SEM, with two-tailed Student's *t*-test. **(J)** Schematic diagram of two classical protein degradation pathways. Treatment with MG132 inhibits proteasome function by blocking its proteolytic activity, and Baf A1 (bafilomycin A1) inhibits autophagy by inhibiting the fusion between autophagosomes and lysosomes (created with BioRender.com). **(K, L)** Western blot analysis of lamin B1 protein in C2C12 seeded onto 0.2 kPa and 10 kPa gels for 0.5 hours in the presence of MG132 (10 μ M). $n = 3$. **(M to O)** Western blot analysis of lamin B1 protein and LC3-II/LC3-I protein in C2C12 seeded onto 0.2 kPa and 10 kPa gels for 0.5 hours in the presence of Baf A1 (100 nM). $n = 3$. **(P)** Immunofluorescence of C2C12 cells on 0.2 kPa substrates for 0.5 hours with DMSO or MG132 or Baf A1 treatment. Hoechst for nuclear staining in blue and lamin B1 staining in green. Scale bars, 4 μ m. **(Q, R)** Quantitative analysis of the fluorescence intensity of lamin B1 **(Q)** and nuclear volume **(R)** for the images from **(P)** (> 50 cells for each condition, One-way ANOVA/Dunnett's multiple comparisons test. Data are presented as the mean \pm SD). Data information: in **(C, E, G, L, Q, R)** as the mean \pm SD, with Two-tailed Student's *t*-test.

Midnolin-proteasome pathway mediates lamin B1 degradation on soft matrix

Given that conventional protein degradation pathways rely on ubiquitination (Pohl & Dikic, 2019), we sought to investigate the mechanoadaptation mechanism underlying lamin B1 degradation on soft matrix. First, we treated C2C12 cells with MG132 and conducted co-immunoprecipitation (Co-IP) analysis. No substantial ubiquitination on lamin B1 protein was detected on soft matrix (Fig. EV3A), implying lamin B1 degradation occurs through ubiquitination-independent proteasomal pathway.

Latest study identified a novel ubiquitin-independent proteasomal degradation pathway mediated by the nuclear protein midnolin (Gu *et al.*, 2023). Midnolin captures proteins through its Catch domain and guides them to proteasomal degradation (Fig. 4A). To determine whether midnolin contributes to lamin B1 degradation, we firstly checked midnolin levels on different stiffness matrix. Our results revealed a significant decrease in midnolin protein levels in C2C12 cells cultured on 0.2 kPa matrix compare to 10 kPa matrix within 30 minutes of seeding. This autoregulatory reduction in midnolin abundance on soft matrix mirrors the mechanosensitive degradation kinetics observed for lamin B1 (Fig. 4B, C). Midnolin knockdown by siRNA significantly elevated lamin B1 levels on 0.2 kPa substrates but no significant effect on 10 kPa substrates, demonstrating that midnolin-mediated lamin B1 degradation is stiffness-dependent (Fig. 4D, E and Fig. EV3B). Immunofluorescence results further confirmed a two-fold increase in lamin B1 levels on soft matrix upon midnolin knockdown compared to the control group (Fig. 4F, G). However, midnolin knockdown did not prevent nuclear volume reduction (Fig. 4F, H), implying other mechanosensitive nuclear morphology involves midnolin-independent pathways, potentially mediated by other NE components.

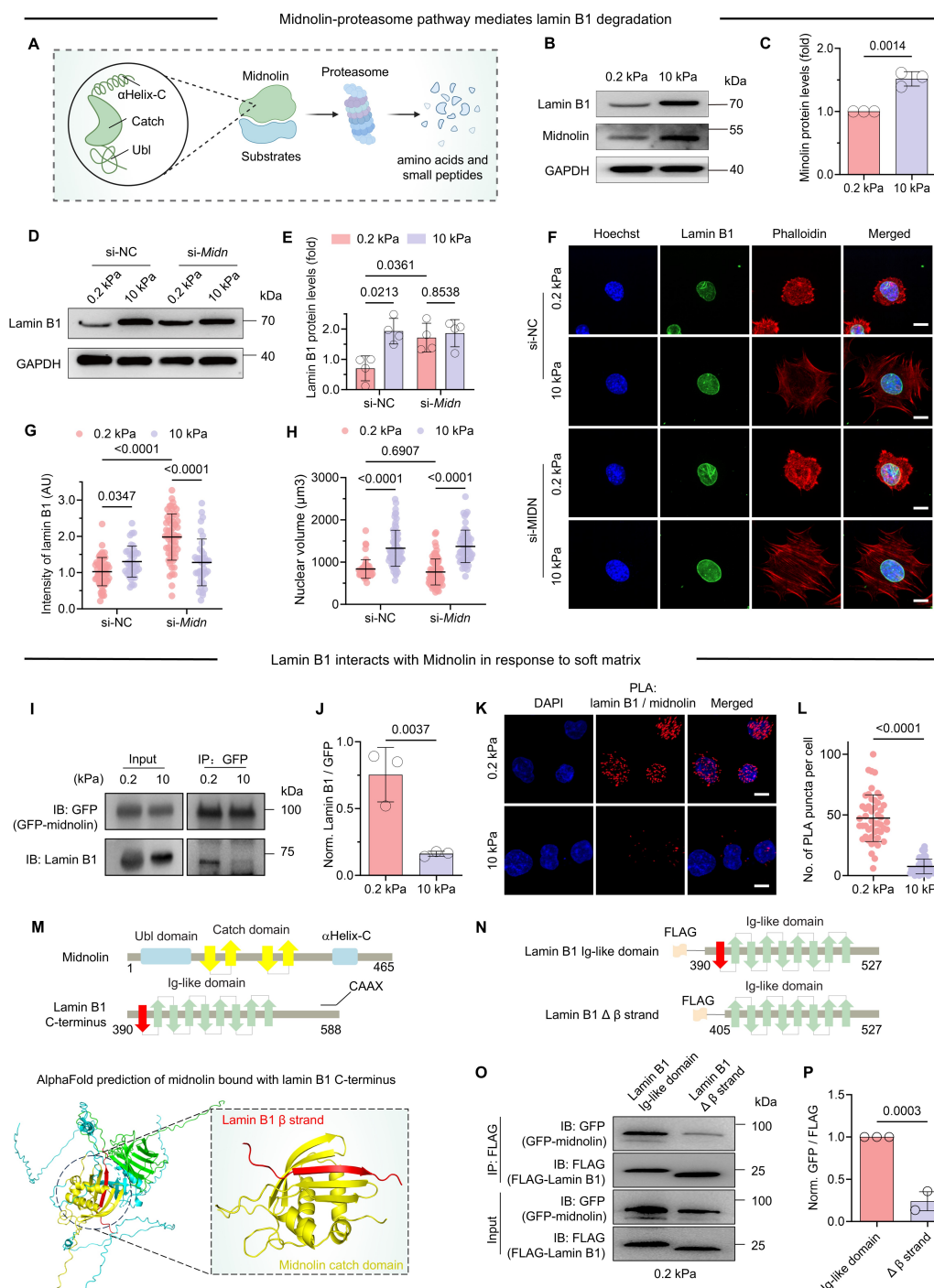


Figure 4. Midnolin-proteasome pathway mediates lamin B1 degradation.

(A) Schematic diagram of midnolin-proteasome pathway: Midnolin contains three main structural domains: the Catch domain, responsible for substrate capture; the C-terminal α Helix-C, binds to the proteasome; and the N-terminal Ubl (ubiquitin-like domain) facilitates substrate degradation. (B, C) Representative western blots and quantification analysis show the protein level changes of midnolin in C2C12 seeding onto 0.2 kPa and 10 kPa gels for 0.5 hours. $n = 3$. (D, E) Representative western blots and quantification data show the recovery of lamin B1 in response to midnolin knockdown by si-Midn in C2C12 after seeding cells on 0.2 kPa and 10 kPa gels for 0.5 hours. $n = 5$. (F) Representative images from negative control scramble siRNA (si-NC) and midnolin knockdown (si-Midn) C2C12 cells seeding on 0.2 kPa and 10 kPa gels for 0.5 hours. Scale bars, 10 μ m. (G, H) Quantification data of lamin B1 intensity (G) and nuclear volume (H) for fluorescence images in (F) (>50 cells for each condition). (I) GFP-midnolin HEK293T cells were pre-treated with MG132 for 3 hours and then plated onto gels for 3 hours, Co-IP analysis to detect the interaction midnolin and lamin B1 was performed. IP and IB both with GFP antibody and lamin B1 antibody. (J) Normalized Lamin B1/GFP intensity in (I). $n = 3$. Data

presented as the mean \pm SD. Two-tailed Student's *t*-test was used for statistical analysis. **(K)** In-cell lamin B1 and GFP-midnolin interactions as demonstrated by Proximity Ligation Assay (PLA) in the nucleus of HEK293T cells with MG132 treatment. PLA was performed on HEK293T cells transfected with GFP-midnolin. Each red dot indicates the protein-protein interaction between GFP-midnolin and endogenous lamin B1. DAPI was used as the nuclear stain. Scale bar: 10 μ m. **(L)** Quantification of PLA signals from experiments as in **(K)** (Two-tailed Student's *t*-test, Data are presented as the mean \pm SD. >50 cells for each condition). **(M)** Schematic representation of midnolin and lamin B1. AlphaFold structure prediction of midnolin bound to its substrate lamin B1 (Ig-like domain) reveals an adopted β -strand capture model. **(N)** Schematics of lamin B1 Ig-like domain and β -strand truncation. **(O)** HEK293T cells were transfected with Lamin B1 Ig-like domain or β -strand truncation and cultured on 0.2 kPa gels for 3 hours. **(P)** Normalized midnolin/lamin B1 intensity in **(O)**. *n* = 3. Data information: in **(C, E, G, H, J, L and P)** were presented as the mean \pm SD. Two-tailed Student's *t*-test was used for statistical analysis for **(C, E, J, L and P)**. Tukey's multiple comparisons test was done for **(G)** and **(H)**.

To further investigated the potential interaction between midnolin and lamin B1, we transiently transfected GFP-midnolin into human embryonic kidney (HEK)-293T cells, and seeded them onto different stiffness matrix. Consistent with observations in C2C12 cells, lamin B1 levels significantly reduced on soft matrix in HEK293T cells (Fig. EV4A, B), suggesting conservation of this mechanoadaptive response across cell types. To study their direct binding, we treated GFP-midnolin overexpressed HEK293T cells with MG132 to stabilize potential transient interactions. Co-IP and immunoblotting assays confirmed that midnolin did interact with lamin B1 specifically on 0.2 kPa matrix but not on 10 kPa matrix (Fig. 4I, J). Additionally, in situ proximity ligation assay (PLA) revealed the interaction between lamin B1 and midnolin in HEK293T cells expressing GFP-midnolin on matrix, with higher PLA signals on 0.2 kPa (Fig. 4K, L). Therefore, both Co-IP and PLA provided the direct evidence for the interaction between midnolin and lamin B1 in those cells on 0.2 kPa matrix. Moreover, super-resolution imaging analysis further showed that the colocalization of midnolin and lamin B1 increased in C2C12 cells after MG132 treatment for 0.5 hours on soft matrix but not on stiff matrix (Fig. EV4C, D).

To elucidate the structural basis of midnolin-lamin B1 interaction, we predict their binding interface through AlphaFold. Notably, the simulation revealed that midnolin's Catch domain specifically recognizes and engages a β -strand within the Ig-like domain of lamin B1, forming a five-stranded antiparallel β -sheet tertiary structure (Fig. 4M). This structural interface precisely matches the reported β -strand capture mechanism of midnolin-mediated proteasomal targeting (Gu *et al.*, 2023). We next performed Co-IP experiments to identify β -stand of lamin B1 that are required for its interaction with midnolin. Deletion of the β -stand of lamin B1 disrupted the stable association of lamin B1 with midnolin on soft matrix (Fig. 4N-P). Notably, deletion of the C-terminal CAAX motif, a membrane-anchoring domain, did not affect lamin B1 binding to midnolin, indicating that this domain is dispensable for their stable interaction (Fig. EV4E-G). Together, these data demonstrate that the degradation of lamin B1 on soft matrix is dependent on midnolin mediated proteasomal degradation pathway.

Loss of lamin B1 attenuates myoblast differentiation

To investigate the functional consequences of midnolin-mediated stiffness-dependent lamin B1

degradation, we first asked whether preventing lamin B1 degradation could rescue muscle atrophy on soft matrix. Knockdown of midnolin in C2C12 cells restored expression of lamin B1 and rescued myoblast differentiation on soft matrix (Fig. 5A-C), demonstrating that lamin B1 degradation is a functional effector of stiffness - dependent differentiation.

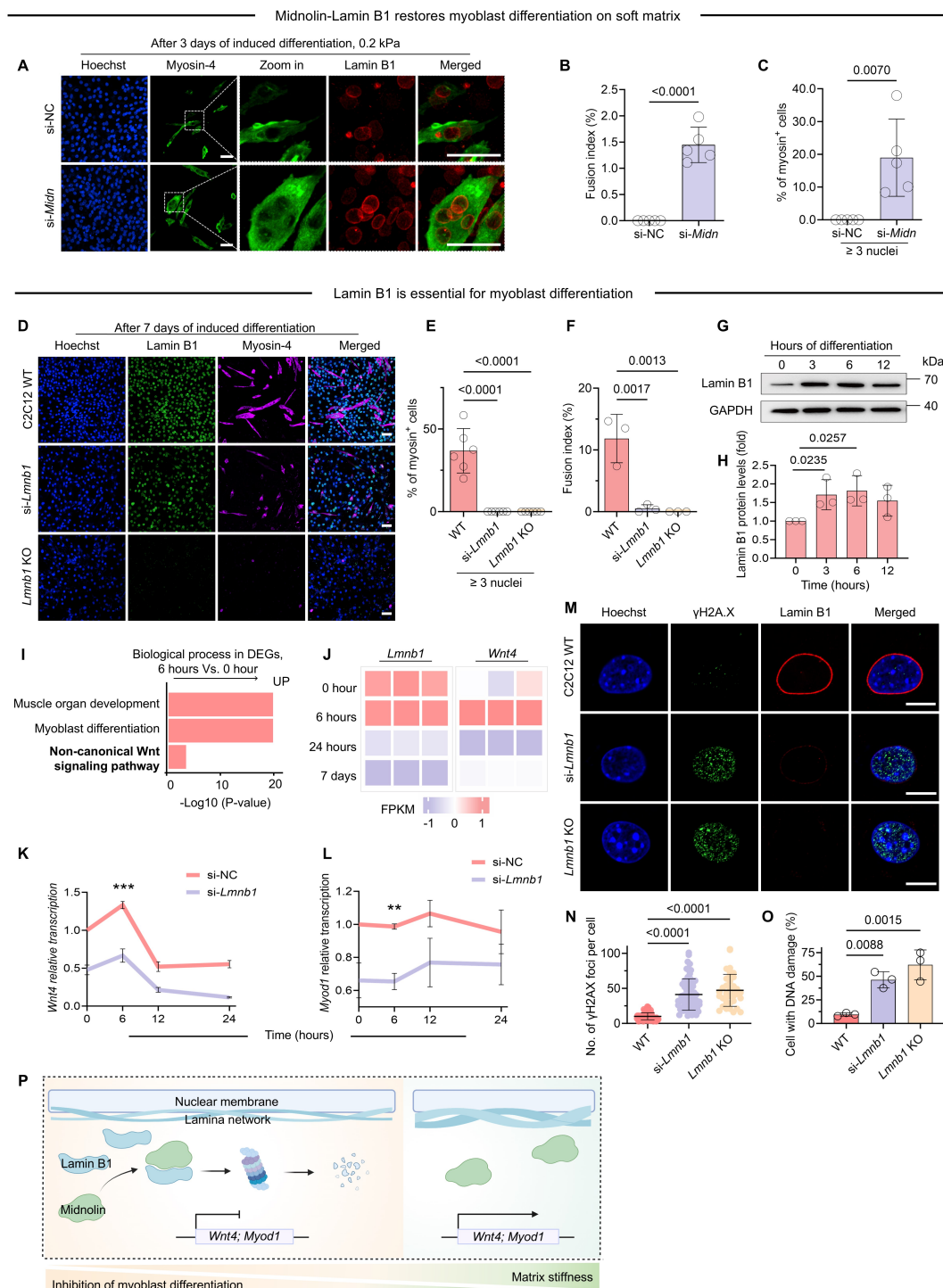


Figure 5. Lamin B1 protein is essential for myoblast differentiation.

(A) Representative images of si-NC and si-Midn C2C12 cells on 0.2 kPa gels show the recovery of myoblast differentiation for 3 days. Scale bar, 50 μ m. (B, C) Quantification data of the fusion index and the percentage of myosin⁺ cells that \geq 3 nuclei in (A). n = 5. Two-tailed Student's *t*-test. (D)

Representative images of WT, si-*Lmnbl*, and *Lmnbl* KO C2C12 cells on petri-dishes with horse serum induced differentiation for 7 days. scale bar, 100 μ m. (E, F) Quantification data of the fusion index and the percentage of myosin⁺ cells that \geq 3 nuclei in (D). One-way ANOVA/Dunnett's multiple comparisons test. (G, H) Western blot analysis of lamin B1 dynamics in C2C12 during 2% horse serum induced differentiation on standard petri-dishes, with corresponding intensity quantification data. n = 3. (I) GO terms analysis of biological processes for upregulated genes (6 hours Vs. 0 hour) after 2% horse serum induced differentiation. (J) Representative genes from RNA-seq were upregulated in pink and downregulated in violet genes after 2% horse serum induced differentiation. (K, L) qPCR to examine the expression of *Wnt4* and *Myod1* during 24 hours differentiation with scramble siRNA (si-NC and si-*Lmnbl*). n = 3. Two-tailed Student's *t*-test. (M) Representative images from WT, si-*Lmnbl*, and *Lmnbl* KO C2C12 cells on petri-dishes after 3 days of horse serum induction. Hoechst for nuclear staining in blue, γ H2AX staining in green and lamin B1 staining in red. Scale bars, 10 μ m. (N, O) The Quantification of DNA damage (M) and γ H2AX foci (L) in (J). n > 40 cells for each condition. One-way ANOVA/Dunnett's multiple comparisons test. (P) Schematic model representation showing that lamin B1 protein levels are reduced by midnolin mediated proteasomal degradation on soft matrix. Consequently, this leads to reduced transcription of *Wnt4* and *Myod1*, which inhibits the process of myoblast differentiation (figure created with BioRender.com). Data information: data in (B, C, E, F, H, K, L, N and O) were presented as the mean \pm SD.

We then examined the potential role of lamin B1 in myoblast differentiation. We directly used siRNA and CRISPR/Cas9 systems to verify the function of lamin B1 in myotube formation. Knockdown of *Lmnbl* reduced myoblast differentiation a lot, while knockout of *Lmnbl* completely abolished myoblast differentiation (Fig. 5D-F). This suggested that lamin B1 is required for myoblast differentiation. Subsequently, we demonstrated lamin B1 protein level indeed dynamically changed during C2C12 differentiation with a significant increase observed within the critical early stage (< 3 hours post-induction), implying its potential role for initiating myoblast differentiation (Fig. 5G, H). To determine its functional effect, GO analysis of upregulated genes identified non-canonical Wnt signaling as an affected pathway during this early stage (Fig. 5I). Further analysis implicated the involvement of *Wnt4*, a known regulator of skeletal muscle development (Takata *et al*, 2007; Tanaka *et al*, 2011), as a key component of these regulatory networks (Fig. 5J). Consistent with these findings, *Lmnbl* knockdown resulted in significantly reduced *Wnt4* expression during differentiation, with the most pronounced decrease occurring at 6 hours post-induction (Fig. 5K and Fig. EV5A). We next examined key myogenic regulator: *Myod1*, which drives differentiation (Olguín & Pisconti, 2012). qPCR analysis showed that *Lmnbl* knockdown caused sustained dysregulation of *Myod1* expression patterns throughout myoblast differentiation (Fig. 5L). Collectively, these results suggested that the decrease of lamin B1 protein attenuates myoblast differentiation through downregulating differentiation-related genes in myoblasts specifically. We next examined whether lamin B1 depletion affects genomic stability during differentiation. Strikingly, *Lmnbl*-deficient C2C12 cells exhibited a significant increase in γ H2AX foci (Fig. 5M-O). These findings suggest that lamin B1 maintains genomic integrity during myogenesis, and its loss leads to both DNA damage accumulation and impaired differentiation. We further generated C2C12 cells stably overexpressing lamin B1, constitutive lamin B1 expression impaired rather than enhanced myoblast differentiation (Fig. EV5B). Time-course analysis revealed that endogenous lamin B1 protein levels progressively declined during prolonged differentiation

(Fig. EV5C, G), suggesting its functional requirement is restricted to early differentiation stages. Taking together, these results demonstrate that lamin B1 mediates stiffness-dependent regulation of myoblast differentiation, where its transient early expression is required for differentiation initiation.

Discussion

Collectively, our data discover that low matrix stiffness induces disruption of nuclear integrity in hindering myoblast differentiation. To elucidate the nuclear skeleton in regulation of nuclear integrity under mechanical stimulation, we observed lamina protein reduction in C2C12 exposed to soft matrix. Notably, we revealed that the transient lamin B1 protein decrease relays on ubiquitination-independent midnolin-proteasome degradation pathway via a β -strand capture mechanism. In addition, the soft matrix-induced lamin B1 degradation impedes myoblast differentiation into myotubes, potentially mediated by reduced expression of *Wnt4* and *Myod1* following lamin B1 knockdown. These results suggest that soft matrix enhances midnolin-lamin B1 interaction to promote lamin B1 proteasomal degradation, leading to nuclear abnormalities, DNA damage, and subsequent repression of *Wnt4* and *Myod1* expression, ultimately impairing myoblast differentiation (Fig. 5P). These data uncover a previously unrecognized relationship whereby matrix stiffness modulates lamin B1 protein levels to govern myoblast differentiation.

Nuclear mechanics has emerged as a central focus in cellular mechanobiology research. Our findings demonstrate that ECM stiffness modulates nuclear lamina organization and transcriptional programs to drive cell fate decisions (Fig. 1), which is consistent with previous reports (De Belly *et al.*, 2022; Nava *et al.*, 2020). People have highlighted the ability of lamin A/C responds to mechanical stimuli at both protein level and spatial location, thereby influences the differentiation of MSCs (Buxboim *et al.*, 2014; Ihalaenen *et al.*, 2015; Swift *et al.*, 2013). In contrast to lamin A/C, lamin B1 - while essential for nuclear membrane integrity - has been primarily characterized for its developmental functions (Chang *et al.*, 2022; Vergnes *et al.*, 2004), with its potential role in nuclear mechanoadaptation and cell fate regulation remaining largely unexplored. Our data show that lamin B1 decreases on soft matrix, inducing nuclear volume shrinkage and envelope wrinkling phenotypically (Fig. 1-2), which is similar to the phenotype in lamin B1 knockout cells reported by previous studies (Vahabikashi *et al.*, 2022). However,

1 the trends in lamin B1 abundance and nuclear volume are not strictly proportional. We speculate
 2 that this imperfect correlation may be attributable to compensatory contributions from
 3 lamin A/C, whose levels and organization are also regulated by ECM stiffness (Fig. 2B). This
 4 interpretation is supported by prior studies demonstrating that lamin A/C and lamin B1
 5 differentially contribute to nuclear architecture and mechanics (Kim *et al*, 2017; Matias *et al*,
 6 2022; Vahabikashi *et al.*, 2022). Although how distinct lamin subtypes coordinately regulate
 7 nuclear mechanical adaptation to ECM cues remains to be elucidated.

8 We also found that appropriate lamin B1 protein levels are critical for early myoblast formation
 9 (Fig. 5), due to the fact that the process of early myoblast differentiation may require nuclear
 10 skeleton remodeling. Previous study showed that both LBR and lamin B2 have a tendency to
 11 be up-regulated in early stage of differentiation followed by gradual decrease (Bakay *et al*,
 12 2006). Another NE protein, Emerin, is required for the perinuclear localization and inhibition
 13 of expression of *Myod1*, *Myf5*, and *Pax7* (Demmerle *et al*, 2013). *Myod1*, a master regulator of
 14 myogenesis, orchestrates myoblast differentiation and exhibits a two-fold upregulation during
 15 this process (Crisp *et al*, 2006). While the regulatory relationship between lamin B1 and
 16 myogenic factors *Myod1* and *Wnt4* has remained unexplored, our study establishes for the first
 17 time that lamin B1 protein levels directly correlate with the dynamics of *Myod1* and *Wnt4*
 18 expression during myoblast differentiation. Reduction of lamin B1 level by soft matrix or direct
 19 deficiency of lamin B1 lead to DNA damage in cells during myogenic differentiation (Fig. 1
 20 and 5). As a previous study reported, in a differentiation checkpoint where genome integrity
 21 needs to be ensured, DNA damage can impede the process of myogenic differentiation (Puri *et al*,
 22 2002).

23 The 'half-life' of different proteins in the cell is quite variable (Correa Marrero & Barrio-
 24 Hernandez, 2021; Eldeeb *et al*, 2019), and this also depends on the types of the stimuli. The
 25 half-life of lamin B1 degradation induced by oncogenic injury is longer than a day via the
 26 autophagy pathway (Dou *et al.*, 2015), whereas the ubiquitination-dependent proteasomal
 27 degradation pathway mediated by E3 ligases also requires a minimum half-life of 6 hours for
 28 lamin B1 (Khanna *et al.*, 2018; Krishnamoorthy *et al.*, 2018). However, our results suggest that
 29 in addition to the lamin B1 degradation process described above, the response of lamin B1 to
 30 mechanical stimuli is dependent on the ubiquitination-independent proteasome pathway (Fig.

1 3 and 4). As latest study reported, midnolin facilitates substrate degradation with its self-
2 contained Ubl domain, which is a much faster pathway to achieve efficient and protein
3 degradation (Gu *et al.*, 2023). We also validated that the interaction between lamin B1 and
4 midnolin followed the mechanism through β strand degron constitution (Fig. 4L). Therefore,
5 midnolin-mediated lamin B1 degradation in response to soft matrix represents a precise
6 molecular mechanism underlying nuclear mechano-adaptation.

7 In summary, we have identified a novel ubiquitination-independent mechanism whereby
8 midnolin targets lamin B1 for proteasomal degradation in response to mechanical cues, leading
9 to nuclear integrity loss. This pathway plays a critical role in myogenesis by modulating the
10 expression of key myogenic regulators *Myod1* and *Wnt4*. Our results establish the midnolin-
11 mediated lamin B1 degradation pathway as a potential therapeutic lever for intervening in
12 muscle pathologies characterized by defective nuclear mechanotransduction.

13

Materials and methods

Table 1. Key resources table

Reagent or resource	Source	Catalog Number
Antibodies		
Rabbit SUN1 (1:1000)	Abcam	Cat#ab103021
Rabbit SUN2 (1:5000)	Abcam	Cat#ab124916
Rabbit KAP1 (1:5000)	Abcam	Cat#ab109287
Rabbit Emerin (1:1000)	Cell Signaling Technology	Cat#30853
Rabbit GAPDH (1:5000)	Cell Signaling Technology	Cat#2118
Rabbit HP1α (1:1000)	Cell Signaling Technology	Cat#2616
Anti-rabbit IgG, HRP-linked Antibody (1:10000)	Cell Signaling Technology	Cat#7074
Anti-mouse IgG, HRP-linked Antibody (1:10000)	Cell Signaling Technology	Cat#7076
Anti-rat IgG, HRP-linked Antibody (1:1000)	Cell Signaling Technology	Cat#7077
Mouse Lamin A/C (1:1000)	Cell Signaling Technology	Cat#4777
Mouse Lamin B Receptor (1:1000)	Abcam	Cat#ab232731
Mouse LAP2 (1:5000)	BD Biosciences	Cat#BD611000
Mouse Myosin 4 (1:1000 for WB, 1:500 for IF)	eBioscience™	Cat#14-6503-82
Mouse Lamin B1 (1:500 for IF)	Santa Cruz Biotechnology	Cat#sc-374015
Rat Nup153 (1:1000)	Santa Cruz Biotechnology	Cat#sc-101544
Anti-mouse IgG (H+L), F(ab')₂ Fragment (Alexa Fluor® 488 Conjugate) (1:1000)	Cell Signaling Technology	Cat#4408
Anti-rabbit IgG (H+L), F(ab')₂ Fragment (Alexa Fluor® 594 Conjugate) (1:1000)	Cell Signaling Technology	Cat#8889
Anti-rabbit IgG (H+L), F(ab')₂ Fragment (Alexa Fluor® 647 Conjugate) (1:1000)	Cell Signaling Technology	Cat#4414
Rabbit Lamin B1 (1:1000)	Abcam	Cat#ab16048
Rabbit ubiquitin (1:1000)	Cell Signaling Technology	Cat#58395S
Rabbit midnolin (1:200)	proteintech	Cat#18939-1-AP
Rabbit γH2AX (1:500)	Beyotime	Cat#C2035S
Mouse puromycin (1:1000)	Merckmillipore	Cat#MABE343
Chemicals		
Cycloheximide	MedChemExpress	Cat#HY-12320
MG132	MedChemExpress	Cat#HY-13259
Bafilomycin A1	MedChemExpress	Cat#HY-100558
DMSO	Solarbio	Cat#D8370

Cell Culture

C2C12 (ATCC, CRL-1772™) and HEK293T (ATCC, CRL-3216™) Cells were propagated in Dulbecco's modified Eagle's medium (DMEM) (Gibco, C11995500) containing 20% Australia origin fetal bovine serum (AFBS) (Sigma, F8318) and 1% penicillin-streptomycin (Gibco, 15140122). Primary myoblasts were a kind gift of Dr. Yang Zhang, and were cultured in Nutrient Mixture F-12 Ham (Sigma, N6658) with 20% AFBS, 5 ng/mL basic FGF (YEASEN, 91330ES10) and 1% penicillin-streptomycin.

Cells differentiated with DMEM containing 2% heat-inactivated horse serum (Gibco, 26050088), and cultured at 37 °C with 5% CO₂.

Western blot

Western blots were implemented following standard procedures. Briefly, cells were seeded and cultured on the plates or PAA gels accordingly in 37°C incubators. After treatment with inhibitors or gels, cells were lysed using RIPA buffer. Following denaturation, lysates were loaded into 10% TGX Stain-Free polyacrylamide gels (Bio-Rad, 1610183) and transferred onto a 0.45 µm PVDF membrane (Immobilon® - P Membrane, IPVH00010). After blocking with 5% non-fat milk (CST, 9999s), the membranes were incubated with primary antibody overnight at 4°C and with the horseradish-peroxidase (HRP)-conjugated secondary antibody for 1 hour at room temperature. ECL Western Blotting Substrate (Epizyme, SQ201) was used to detect HRP and the bands were visualized with the ChemiDoc MP imaging system (Bio-Rad). The intensity of the bands was analyzed using ImageJ software.

Immunofluorescence

0.1 million C2C12 cells were seeded for staining experiments or 0.3 million C2C12 cells were used for myotube differentiation experiments on fibronectin (Corning, 356008) coated PAA gels or dishes. They were then fixed with 4% Paraformaldehyde (Biosharp, BL539A) for 30 mins at room temperature. 0.25% Triton X-100 (Sangon Biotech, A110694) was used to permeabilize the cells for 15 mins and block with 5% BSA/PBST for 1 hour. Different combinations of the following primary antibodies were then used: mouse anti-Lamin B1 (1:500 Santa Cruz Biotechnology), Rabbit anti-Lamin B1 (1:1000 Abcam), and mouse anti myosin4 (1:100 eBioscience™). Cells were incubated with primary antibodies overnight at 4°C. They were then washed three times with TBST for 10 mins. Then, the gels or dishes were incubated with secondary antibodies at room temperature for 1 hour. They were then stained against Hoechst33342 (CST, 4082) or Alexa Fluor™ 568 phalloidin (ThermoFisher, A12380), and washed again with TBST. The gels were then mounted with VECTASHIELD® Antifade Mounting Medium (Vectorlabs, H-1000).

Preparation of polyacrylamide gels and stiffness measurement

PAA gels were prepared as described previously (Tse & Engler, 2010). Briefly, Different concentrations of acrylamide and bis-acrylamide were mixed in a solution to produce gels of different rigidity. The solution also contained 10% Ammonium persulfate (APS) (Sangon Biotech, A100486), and N, N, N', N'-Tetramethylethylenediamine (TEMED) (Sangon Biotech, A610508). The solution was then placed on top of the glass and covered with a coverslip. After 30 mins, the coverslip was removed with Dulbecco's Phosphate-Buffered Salines (DPBS), and the gels were coated with 20 µg/mL fibronectin overnight at 4°C. After washing gels with PBST, cells were seeded on gels. To perform atomic force microscopy (AFM) measurements, a 1 µm diameter silica colloid was glued onto silicon nitride cantilever (MLCT-O10, Bruker AFM Probes), which was then mounted on a NanoWizard ULTRA Speed 2 system (Bruker). The stiffness was calibrated by determining a spring constant of the cantilever from the thermal fluctuations at room temperature, ranging from 0.01~1 N/m. The cantilever was moved towards the stage at a rate of 1 µm s⁻¹ for indentations.

Co-immunoprecipitation (Co-IP) assays

Co-IP was conducted as previously described (Tang *et al*, 2022). Briefly, HEK293T cells were transfected with GFP-midnolin using Lipofectamine 3000 reagent (Invitrogen™, L3000001). After

transfection 36 hours, cells were treated with MG132 for 6 hours then seeded onto gels for 3 hours. Cells were then washed twice with ice-cold PBS and lysed with IP lysis buffer (Thermo, 87787) containing 100×protease inhibitor (Roche, 11836170001) for 20 mins on ice. After centrifugation at 4°C, 12,000 rpm for 10 mins, the protein supernatant was incubated separately with antibodies against GFP (CST, 2956), lamin B1 (Abcam, 16048) and rabbit IgG (CST, 2729) at 4 °C overnight with rotation. The immune complexes were then incubated with Protein A/G Magnetic Beads (Vazyme, PB101) for 1 hour at room temperature with rotation. For exogenous Co-immunoprecipitation (Co-IP), HEK293T cells transfected with plasmid expressing Flag-lamin B1, the supernatants mixed with Anti-Flag Nanobody-Magarose Beads (AlpaLifeBio, KTSM1361) were rotated for 2 hrs at 4 °C. After placing the tube on a magnet to separate the beads from the solution, the supernatant was removed, and the beads were washed three times with lysis wash buffer. Finally, 2×SDS loading buffer was added to each sample for subsequent western blot analysis.

In vivo ubiquitination assay

C2C12 cells were seeded on gels for 30 mins, and then lysed using the IP lysis buffer containing 100×protease inhibitor (Roche, 11836170001) and 5 mM/L N-ethylmaleimide (MedChemExpress, HY-D0843) to prevent de-ubiquitylation for 30 mins on ice. The cell lysates were immunoprecipitated using the antibodies against lamin B1 (Abcam, 16048) and rabbit IgG, and were then subjected to immunoblotting analysis using antibody against Ub (CST, 3933S).

Proximity ligation assay (PLA)

GFP-midnolin overexpression HEK293T Cells were fixed and permeabilized as described for IF analysis. The assays were carried out using a Duolink PLA kit (Sigma-Aldrich, DUO92002 & DUO92004) following the manufacturer's protocol. Briefly, blocking solution was added for 1 hour at 37°C. Then incubated with primary antibodies overnight at 4°C. Each incubation step was followed by washing 2×5 mins in Duolink® In Situ Wash Buffer. PLA probes (PLUS and MINUS) were added and incubated for 1 hour at 37°C. Ligase solution was then added and incubated for 30 mins at 37°C followed by incubation with amplification solution containing polymerase for 100 mins at 37°C and protected from light. The samples were then mounted with Duolink® In Situ Mounting Medium with DAPI (Sigma-Aldrich, DUO82040).

Super-resolution imaging and data analysis

Cells were fixed and prepared as IF described above, and imaging was conducted using a ZEISS Elyra 7 equipped with a 100×/1.46 NA oil immersion objective. Samples were excited with 488 nm and 561 nm lasers, and structured illumination microscopy (SIM) mode was used for reconstruction. All images were processed with ZEISS ZEN software using consistent parameters, including 3D SIM reconstruction, noise filtering, and alignment, to ensure reproducibility. The Pearson's coefficients were rigorously calculated from ≥ 5 cells per condition using Imaris software, analyzing colocalization specifically within nuclear volumes while applying consistent thresholding and background subtraction parameters.

Cell transfection

Plasmid DNA transfection was performed using Lipofectamine 3000 reagent (Invitrogen, L3000001), whereas siRNA transfection was performed using Lipofectamine RNAiMax (Invitrogen, 13778075). All experiments were performed 48 hours after transfection.

The siRNA oligonucleotides for negative control: 5'-UUCUCCGAACGUGUCACGUTT-3' and 5'-ACGUGACACGUUCGGAGAATT-3', *Lmnbl*: 5'-AGAGUCUAGAGCAUGUUUG-3' and 5'-UUCAAGCGAAUAAACUUCCTT-3', *Midn*: 5'-GGAACAGUCCGUUAUGCAATT-3' and 5'-UUGCAUAACGGACUGUUCCTT-3'.

RNA isolation and qPCR

Total RNAs were extracted from cultured C2C12 cells using E.Z.N.A. Total RNA Kit I reagent (Omegabiotek, R6834-01) according to the manufacturer's instructions. Isolated RNAs were reversed-transcribed into cDNA with 5 x PrimeScript RT Master Mix (Takara, RR036A). qPCR (Quantitative real-time-polymerase chain reaction) was performed with Hieff® qPCR SYBR Green Master Mix (Yeast, 11204ES) by using the specific primer pairs. Gene expression was normalized against *GAPDH*. The qPCR primers for *GAPDH* gene were: Forward 5'-CAGAAGACTGTGGATGGCCC-3' and Reverse 5'-ATCCACGACGGACACATTGG-3'; *Lmnbl* gene: Forward 5'-AAGGCTCTCTACGAGACCGA-3' and Reverse 5'-TGATCTGGGCTCCACTGAGA-3'; *Myod1* gene: Forward 5'-TACAGTGGCGACTCAGATGC-3' and Reverse 5'-GTAGTAGGCGGTGTCGTAGC-3'; *Midn* gene: Forward 5'-GCGTCAACTTGCTCCCAT-3' and Reverse 5'-AACGCCTCAAAGTACCCAAG-3'. *Wnt4* gene: Forward 5'-AAGAGGAGACGTGCGAGAAAC-3' and Reverse 5'-GTCCCTTGTCACACCTT-3'. Samples were run on a QuantStudio 3 Real-time PCR System (Applied Biosystems).

CRISPR-mediated lamin B1 gene knockout

To knockout lamin B1 genes, we first inserted *mLmnbl* gRNA into pSpCas9(BB)-2A-GFP (PX458) (addgene#48138). Here we designed primers for two gRNAs (gRNA1: 5' TGCAGGCGCGACAGGCGCGT 3', gRNA2: 5' TCTGGAGCTTGCGCGCTCG 3') and did cloning by using Golden Gate assembly. Plasmids were verified by Sanger sequencing. Then, 0.4 million C2C12 cells were seeded into 6-well plate the day before transfection. 1.25 µg/mL *Lmnbl*-PX458-gRNA1 and 1.25 µg/mL *Lmnbl*-PX458-gRNA2 were co-transfected into C2C12 with Lipofectamine™ 3000 Reagent. 48 hours post-transfection, cells were subjected to FACS to isolate GFP positive single cell clone into 96-well plates. After incubation for about a month, single clone got expanded and verified by genotyping PCR with lamin B1-specific primers (*mLmnbl*-F: 5' GCCTGTGGTTTGTACCTTCG 3', *mLmnbl*-R: 5' TCATTCTTCGGGCCGTTGG 3') as well as Sanger sequencing.

RNA-sequencing

C2C12 cells were treated and sorted as described above to harvest the total RNAs. The RNA integrity was evaluated using the Agilent 2100 Bioanalyzer. Library preparation and sequencing were performed on the Illumina HiSeq 2000 platform. The RNA reads were processed using Ktrim(Sun, 2020) to remove adapters and filter low-quality reads. The processed reads were then aligned to the GRCm38 reference genome using HISAT2 software (Kim *et al*, 2015). Expression quantification was performed using the StringTie software(Pertea *et al*, 2015) against gene annotation obtained from *Mus musculus* Ensembl release 104 (Aken *et al*, 2016). Differential expression analysis was conducted using the DESeq2 tool (Love *et al*, 2014). Only genes with a fold change greater than 2 and an adjusted *p*-value less than 0.05 were considered differentially regulated. The bioinformatics resources of the Database for Annotation,

Visualization, and Integrated Discovery (DAVID)(Dennis *et al*, 2003) were used for functional annotation enrichment analysis of differentially expressed genes.

Prediction of the interaction between lamin B1 and midnolin by AlphaFold

Residues 390-588 of *Lmnbl* sequence (UniProtKB: P14733) was paired with the MIDN sequence (UniProtKB: Q3TPJ7) as the input for multimer prediction by using AlphaFold (v2.3.2). Default reference databases and max_template_data = 2024-04-05 were used during structure prediction. We ran 10 independent predictions, and selected the top-ranking model based on the iptm+ptm score.

Plasmid cloning

The cDNA sequences of lamin B1 were cloned into the pSIN-FLAG vector. Various truncations (Δ β -strand, residues 390 to 404; Δ CAAX motif, residues 527 to 588;) of lamin B1 were generated from the pSIN-FLAG-lamin B1 construct to facilitate direct transfection. All newly created constructs in this study were rigorously verified through DNA sequencing to ensure their accuracy and integrity.

Puromycin incorporation assay

Puromycin incorporation assay was performed as described (Zhang *et al*, 2018). C2C12 cells were treated with 91 μ M puromycin for 5 minutes after plating onto gels 25 minutes. Whole cell lysates were analyzed by Western Blot using a puromycin antibody (Millipore).

Statistical analysis

All data were obtained from at least three independent experiments unless indicated otherwise. GraphPad Prism 9.0.0 (GraphPad Software) was used for statistical analysis. To calculate Pearson's correlation coefficient, the images were processed by Zeiss Elyra7 SIM (Structured Illumination Microscopy) and then analyzed by Imaris (Microscopy Image Analysis Software) for 3D co-localization. The sample size, statistical significance value and error bar graphs were indicated in figure legends.

Acknowledgments

This work was financially supported by the National Natural Science Foundation of China (32471370 to Q.P., 12372302 to J.Q., 32271360 to Q.L.), the Guangdong Pearl River Talent Program (2021QN02Y781 to Q.P.) and the Natural Science Foundation of Guangdong Province, China (2023A1515010829 to Q.L.). We thank the Bioimaging Core facility at Shenzhen Bay Laboratory for providing imaging support, specifically thanking engineers Mei Yu and Shixian Huang for assistance with Super-Resolution Microscopes (Zeiss Elyra 7) and Dragonfly Spinning Disk Confocal Microscopy (4-laser). We also acknowledge the usage of BioRender (biorender.com) for creating the figures.

Abbreviations

PAA: polyacrylamide; ECM: extracellular matrix; LINC: the linker of nucleoskeleton and cytoskeleton complex; FN: fibronectin; NE: nuclear envelope; NUP153: Nucleoporin 153; LBR: lamin B receptor; LAP2: lamina associated protein 2; ANOVA: analysis of variance; AU: arbitrary unit; CHX: cycloheximide; PLA: proximity ligation assay; MHC: myosin heavy chain; γ H2AX: phosphorylated H2AX at Ser139.

Author contributions

1 **Liping Guo:** Conceptualization; Data curation; Formal analysis; Validation; Visualization;
 2 Methodology; Writing-original draft; Writing-review and editing. **Yanjing Zhao:** Data curation; Formal
 3 analysis; Visualization; Methodology; Writing-review and editing. **Zhe Zhang:** Methodology;
 4 Visualization. **Chang Sun:** Visualization; Writing-review and editing. **Yafan Xie:** Formal analysis;
 5 Visualization, **Qin Dai:** Data curation. **Yaoqi Zhou:** Resources. **Yan Yan:** Resources. **Yang Zhang:**
 6 Resources. **Quhuan Li:** Supervision; Writing-review and editing; Funding acquisition. **Juhui Qiu:**
 7 Conceptualization; Supervision; Funding acquisition; Methodology; Writing-review and editing. **Qin**
 8 **Peng:** Conceptualization; Supervision; Funding acquisition; Methodology; Writing-review and editing.

9

10 **Declaration of interests**

11 The authors declare no competing interests.

12

References

- Aken BL, Ayling S, Barrell D, Clarke L, Curwen V, Fairley S, Fernandez Banet J, Billis K, García Girón C, Hourlier T *et al* (2016) The Ensembl gene annotation system. *Database (Oxford)* 2016
- Baghdadi MB, Houtekamer RM, Perrin L, Rao-Bhatia A, Whelen M, Decker L, Bergert M, Pérez-González C, Bouras R, Gropplero G *et al* (2024) PIEZO-dependent mechanosensing is essential for intestinal stem cell fate decision and maintenance. *Science* 386: eadj7615
- Bakay M, Wang Z, Melcon G, Schiltz L, Xuan J, Zhao P, Sartorelli V, Seo J, Pegoraro E, Angelini C *et al* (2006) Nuclear envelope dystrophies show a transcriptional fingerprint suggesting disruption of Rb-MyoD pathways in muscle regeneration. *Brain* 129: 996-1013
- Balchin D, Hayer-Hartl M, Hartl FU (2016) In vivo aspects of protein folding and quality control. *Science* 353: aac4354
- Beedle AE, Roca-Cusachs P (2023) The reversibility of cellular mechano-activation. *Curr Opin Cell Biol* 84: 102229
- Buxboim A, Swift J, Irianto J, Spinler KR, Dingal PC, Athirasala A, Kao YR, Cho S, Harada T, Shin JW *et al* (2014) Matrix elasticity regulates lamin-A,C phosphorylation and turnover with feedback to actomyosin. *Curr Biol* 24: 1909-1917
- Chang L, Li M, Shao S, Li C, Ai S, Xue B, Hou Y, Zhang Y, Li R, Fan X *et al* (2022) Nuclear peripheral chromatin-lamin B1 interaction is required for global integrity of chromatin architecture and dynamics in human cells. *Protein Cell* 13: 258-280
- Correa Marrero M, Barrio-Hernandez I (2021) Toward Understanding the Biochemical Determinants of Protein Degradation Rates. *ACS Omega* 6: 5091-5100
- Cosgrove BD, Loebel C, Driscoll TP, Tsintman TK, Dai EN, Heo SJ, Dymant NA, Burdick JA, Mauck RL (2021) Nuclear envelope wrinkling predicts mesenchymal progenitor cell mechano-response in 2D and 3D microenvironments. *Biomaterials* 270: 120662
- Crisp M, Liu Q, Roux K, Rattner JB, Shanahan C, Burke B, Stahl PD, Hodzic D (2006) Coupling of the nucleus and cytoplasm: role of the LINC complex. *J Cell Biol* 172: 41-53
- De Belly H, Paluch EK, Chalut KJ (2022) Interplay between mechanics and signalling in regulating cell fate. *Nat Rev Mol Cell Biol* 23: 465-480
- Demmerle J, Koch AJ, Holaska JM (2013) Emerin and histone deacetylase 3 (HDAC3) cooperatively regulate expression and nuclear positions of MyoD, Myf5, and Pax7 genes during myogenesis. *Chromosome Res* 21: 765-779
- Dennis G, Sherman BT, Hosack DA, Yang J, Gao W, Lane HC, Lempicki RA (2003) DAVID: Database for Annotation, Visualization, and Integrated Discovery. *Genome Biol* 4: R60
- Donnalaja F, Jacchetti E, Soncini M, Raimondi MT (2019) Mechanosensing at the Nuclear Envelope by Nuclear Pore Complex Stretch Activation and Its Effect in Physiology and Pathology. *Front Physiol* 10: 896
- Dou Z, Xu C, Donahue G, Shimi T, Pan JA, Zhu J, Ivanov A, Capell BC, Drake AM, Shah PP *et al* (2015) Autophagy mediates degradation of nuclear lamina. *Nature* 527: 105-109
- Dupont S, Wickstrom SA (2022) Mechanical regulation of chromatin and transcription. *Nat Rev Genet* 23: 624-643
- Echarri A, Pavón DM, Sánchez S, García-García M, Calvo E, Huerta-López C, Velázquez-Carreras D, Viaris de Lesegno C, Ariotti N, Lázaro-Carrillo A *et al* (2019) An Abl-FBP17 mechanosensing system couples local plasma membrane curvature and stress fiber remodeling during mechanoadaptation. *Nat Commun* 10: 5828

- 1 Eldeeb MA, Siva-Piragasam R, Ragheb MA, Esmaili M, Salla M, Fahlman RP (2019) A molecular
2 toolbox for studying protein degradation in mammalian cells. *J Neurochem* 151: 520-533
- 3 Fiore VF, Almagro J, Fuchs E (2025) Shaping epithelial tissues by stem cell mechanics in development
4 and cancer. *Nat Rev Mol Cell Biol* 26: 442-455
- 5 Gibbons MC, Singh A, Engler AJ, Ward SR (2018) The role of mechanobiology in progression of
6 rotator cuff muscle atrophy and degeneration. *J Orthop Res* 36: 546-556
- 7 Gu X, Nardone C, Kamitaki N, Mao A, Elledge SJ, Greenberg ME (2023) The midnolin-proteasome
8 pathway catches proteins for ubiquitination-independent degradation. *Science* 381: eadh5021
- 9 Ihalaainen TO, Aires L, Herzog FA, Schwartlander R, Moeller J, Vogel V (2015) Differential basal-to-
10 apical accessibility of lamin A/C epitopes in the nuclear lamina regulated by changes in cytoskeletal
11 tension. *Nat Mater* 14: 1252-1261
- 12 Kalukula Y, Stephens AD, Lammerding J, Gabriele S (2022) Mechanics and functional consequences
13 of nuclear deformations. *Nat Rev Mol Cell Biol* 23: 583-602
- 14 Khanna R, Krishnamoorthy V, Parnaik VK (2018) E3 ubiquitin ligase RNF123 targets lamin B1 and
15 lamin-binding proteins. *FEBS J* 285: 2243-2262
- 16 Kim D, Langmead B, Salzberg SL (2015) HISAT: a fast spliced aligner with low memory
17 requirements. *Nat Methods* 12: 357-360
- 18 Kim JK, Louhghalam A, Lee G, Schafer BW, Wirtz D, Kim DH (2017) Nuclear lamin A/C harnesses
19 the perinuclear apical actin cables to protect nuclear morphology. *Nat Commun* 8: 2123
- 20 Kjaer M (2004) Role of extracellular matrix in adaptation of tendon and skeletal muscle to mechanical
21 loading. *Physiol Rev* 84: 649-698
- 22 Krishnamoorthy V, Khanna R, Parnaik VK (2018) E3 ubiquitin ligase HECW2 targets PCNA and
23 lamin B1. *Biochim Biophys Acta Mol Cell Res* 1865: 1088-1104
- 24 Long AM, Kwon JM, Lee G, Reiser NL, Vaught LA, O'Brien JG, Page PGT, Hadhazy M, Reynolds
25 JC, Crosbie RH *et al* (2024) The extracellular matrix differentially directs myoblast motility and
26 differentiation in distinct forms of muscular dystrophy: Dystrophic matrices alter myoblast motility.
27 *Matrix biology : journal of the International Society for Matrix Biology* 129: 44-58
- 28 Love MI, Huber W, Anders S (2014) Moderated estimation of fold change and dispersion for RNA-seq
29 data with DESeq2. *Genome Biol* 15: 550
- 30 Lovett DB, Shekhar N, Nickerson JA, Roux KJ, Lele TP (2013) Modulation of Nuclear Shape by
31 Substrate Rigidity. *Cell Mol Bioeng* 6: 230-238
- 32 Matias I, Diniz LP, Damico IV, Araujo APB, Neves LDS, Vargas G, Leite REP, Suemoto CK, Nitrini
33 R, Jacob-Filho W *et al* (2022) Loss of lamin-B1 and defective nuclear morphology are hallmarks of
34 astrocyte senescence in vitro and in the aging human hippocampus. *Aging Cell* 21: e13521
- 35 Maurer M, Lammerding J (2019) The Driving Force: Nuclear Mechanotransduction in Cellular
36 Function, Fate, and Disease. *Annu Rev Biomed Eng* 21: 443-468
- 37 Nava MM, Miroshnikova YA, Biggs LC, Whitefield DB, Metge F, Boucas J, Vihinen H, Jokitalo E, Li
38 X, Garcia Arcos JM *et al* (2020) Heterochromatin-Driven Nuclear Softening Protects the Genome
39 against Mechanical Stress-Induced Damage. *Cell* 181: 800-817 e822
- 40 Nguyen J, Wang L, Lei W, Hu Y, Gulati N, Chavez-Madero C, Ahn H, Ginsberg HJ, Krawetz R,
41 Brandt M *et al* (2024) Culture substrate stiffness impacts human myoblast contractility-dependent
42 proliferation and nuclear envelope wrinkling. *J Cell Sci*
- 43 Olguín HC, Pisconti A (2012) Marking the tempo for myogenesis: Pax7 and the regulation of muscle
44 stem cell fate decisions. *J Cell Mol Med* 16: 1013-1025

1 Perteu M, Perteu GM, Antonescu CM, Chang T-C, Mendell JT, Salzberg SL (2015) StringTie enables
2 improved reconstruction of a transcriptome from RNA-seq reads. *Nat Biotechnol* 33: 290-295

3 Pohl C, Dikic I (2019) Cellular quality control by the ubiquitin-proteasome system and autophagy.
4 *Science* 366: 818-822

5 Price AJ, Huang EY, Sebastiano V, Dunn AR (2017) A semi-interpenetrating network of
6 polyacrylamide and recombinant basement membrane allows pluripotent cell culture in a soft,
7 ligand-rich microenvironment. *Biomaterials* 121: 179-192

8 Puri PL, Bhakta K, Wood LD, Costanzo A, Zhu J, Wang JYJ (2002) A myogenic differentiation
9 checkpoint activated by genotoxic stress. *Nat Genet* 32: 585-593

10 Shiraishi K, Shah PP, Morley MP, Loebel C, Santini GT, Katzen J, Basil MC, Lin SM, Planer JD,
11 Cantu E *et al* (2023) Biophysical forces mediated by respiration maintain lung alveolar epithelial
12 cell fate. *Cell* 186: 1478-1492.e1415

13 Sun K (2020) Ktrim: an extra-fast and accurate adapter- and quality-trimmer for sequencing data.
14 *Bioinformatics* 36: 3561-3562

15 Swift J, Ivanovska IL, Buxboim A, Harada T, Dingal PC, Pinter J, Pajeroski JD, Spinler KR, Shin
16 JW, Tewari M *et al* (2013) Nuclear lamin-A scales with tissue stiffness and enhances matrix-
17 directed differentiation. *Science* 341: 1240104

18 Takata H, Terada K, Oka H, Sunada Y, Moriguchi T, Nohno T (2007) Involvement of Wnt4 signaling
19 during myogenic proliferation and differentiation of skeletal muscle. *Developmental dynamics : an*
20 *official publication of the American Association of Anatomists* 236: 2800-2807

21 Tanaka S, Terada K, Nohno T (2011) Canonical Wnt signaling is involved in switching from cell
22 proliferation to myogenic differentiation of mouse myoblast cells. *Journal of molecular signaling* 6:
23 12

24 Tang Y, Jia Y, Fan L, Liu H, Zhou Y, Wang M, Liu Y, Zhu J, Pang W, Zhou J (2022) MFN2 Prevents
25 Neointimal Hyperplasia in Vein Grafts via Destabilizing PFK1. *Circ Res* 130: e26-e43

26 Thomas K, Engler AJ, Meyer GA (2015) Extracellular matrix regulation in the muscle satellite cell
27 niche. *Connect Tissue Res* 56: 1-8

28 Tse JR, Engler AJ (2010) Preparation of hydrogel substrates with tunable mechanical properties. *Curr*
29 *Protoc Cell Biol* Chapter 10: Unit 10.16

30 Vahabikashi A, Sivagurunathan S, Nicdao FAS, Han YL, Park CY, Kittisopikul M, Wong X, Tran JR,
31 Gundersen GG, Reddy KL *et al* (2022) Nuclear lamin isoforms differentially contribute to LINC
32 complex-dependent nucleocytoskeletal coupling and whole-cell mechanics. *Proc Natl Acad Sci U S*
33 *A* 119: e2121816119

34 Vergnes L, Péterfy M, Bergo MO, Young SG, Reue K (2004) Lamin B1 is required for mouse
35 development and nuclear integrity. *Proc Natl Acad Sci U S A* 101: 10428-10433

36 Viridi JK, Pethe P (2022) Soft substrate maintains stemness and pluripotent stem cell-like phenotype of
37 human embryonic stem cells under defined culture conditions. *Cytotechnology* 74: 479-489

38 Wall BT, Dirks ML, van Loon LJC (2013) Skeletal muscle atrophy during short-term disuse:
39 implications for age-related sarcopenia. *Ageing Res Rev* 12: 898-906

40 Wintner O, Hirsch-Attas N, Schlossberg M, Brofman F, Friedman R, Kupervaser M, Kitsberg D,
41 Buxboim A (2020) A Unified Linear Viscoelastic Model of the Cell Nucleus Defines the
42 Mechanical Contributions of Lamins and Chromatin. *Adv Sci (Weinh)* 7: 1901222

1 Zhang K, Daigle JG, Cunningham KM, Coyne AN, Ruan K, Grima JC, Bowen KE, Wadhwa H, Yang
2 P, Rigo F *et al* (2018) Stress Granule Assembly Disrupts Nucleocytoplasmic Transport. *Cell* 173:
3 958-971.e917
4 Zhang W, Liu Y, Zhang H (2021) Extracellular matrix: an important regulator of cell functions and
5 skeletal muscle development. *Cell Biosci* 11: 65
6
7

Expanded View Figures

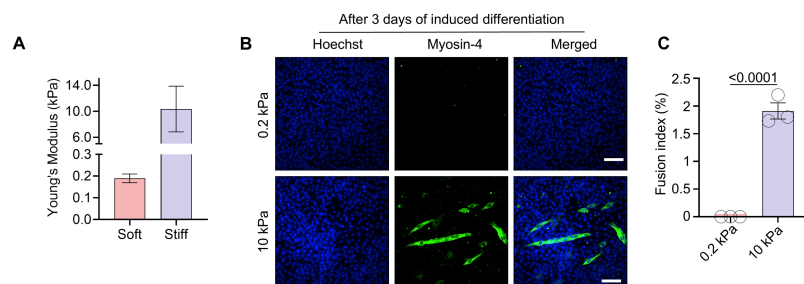


Figure EV1. Young's modulus of PAA gels and early myoblast differentiation on different matrix.

(A) Young's modulus (E, kPa) of PAA hydrogels coated with FN (n = 3 biological replicates). (B) Representative images of differentiated C2C12 cells on 0.2 kPa and 10 kPa matrices after 3 days of 2% horse serum induction. scale bar, 100 μ m. (C) Quantification data of the fusion index in (C). n = 3, Data are presented as the mean \pm SD. Two-tailed Student's *t*-test.

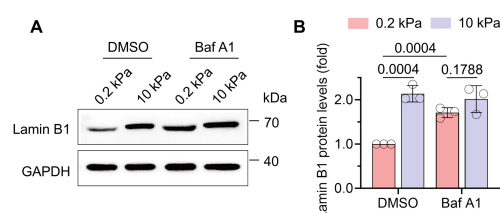


Figure EV2. Bafilomycin A1 treatment on matrix.

(A, B) Western blot analysis of lamin B1 protein in C2C12 seeded onto gels for 30min in the presence of degradation inhibitor (Baf A1, 100 μ M). n = 3, Data are presented as the mean \pm SD. Two-tailed Student's *t*-test.

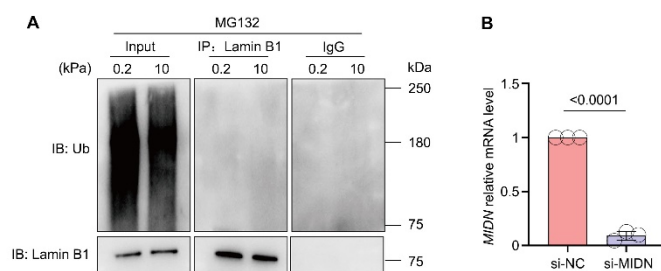


Figure EV3. Ubiquitination assay of lamin B1 protein and qPCR assay of *Midn*.

(A) The ubiquitination level of lamin B1 in C2C12 with MG132. Cells were pre-treated with MG132 for 6 hours and seeded on gels for 0.5 hours, the cells were then harvested with IP lysis buffer. IP assay was performed with anti-ubiquitin. (B) qRT-PCR to detect the expression of *Midn* transduced with si-*Midn*. n = 3. Data are presented as the mean \pm SD. Two-tailed Student's *t*-test was used for statistical analysis.

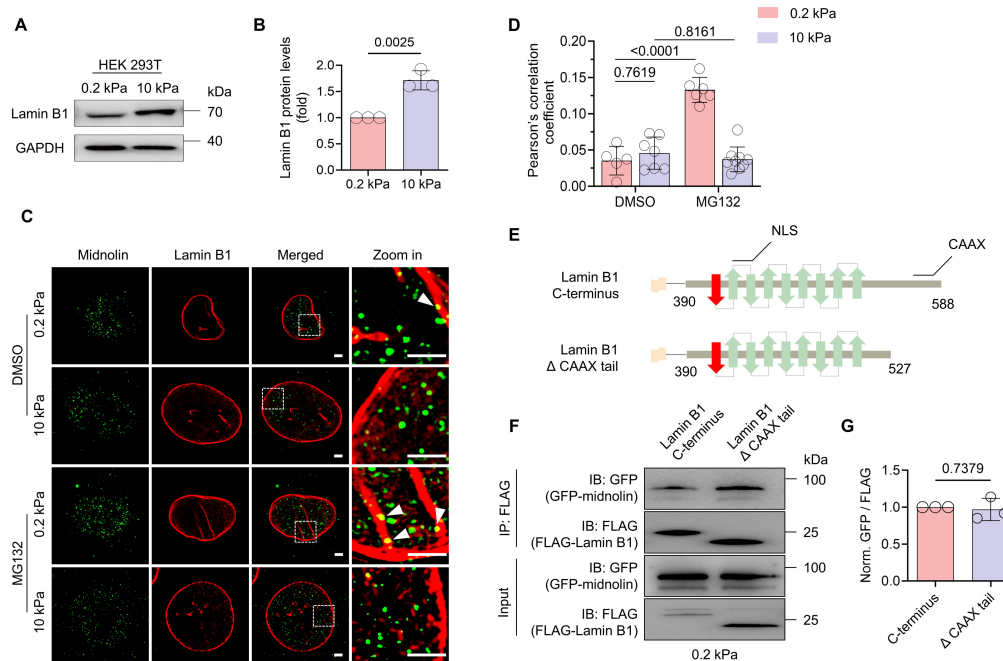


Figure EV4. Lamin B1 interacts with midnolin independent on C terminal tail on 0.2 kPa.

(A, B) Western blot analysis of lamin B1 proteins in HEK293T cells seeded onto 0.2 kPa and 10 kPa gels after 0.5 hours. $n = 3$. (C) Representative SIM images of midnolin (green) and lamin B1 (red) in C2C12 cells on 0.2 kPa and 10 kPa gels with DMSO or MG132 treatment for 0.5 hours. The yellow dots are the colocalization of midnolin and lamin B1 (white arrows). Scale bars, 2 μ m. (D) Pearson's correlation coefficient was calculated for lamin B1 and midnolin based on the imaging results in (C). $n > 5$ cells for each condition. (E) Schematics of lamin B1 Ig-like domain and CAAX motif truncation. (F) HEK293T cells were transfected with Lamin B1 Ig-like domain or CAAX motif truncation and cultured on 0.2 kPa gels for 3 hours. (G) Normalized midnolin / lamin B1 intensity in (F). $n = 3$. Data (B, C and G) are the mean \pm SD, with Two-tailed Student's t -test.

Figure S4. Myoblast differentiation requires moderate lamin B1 protein levels.

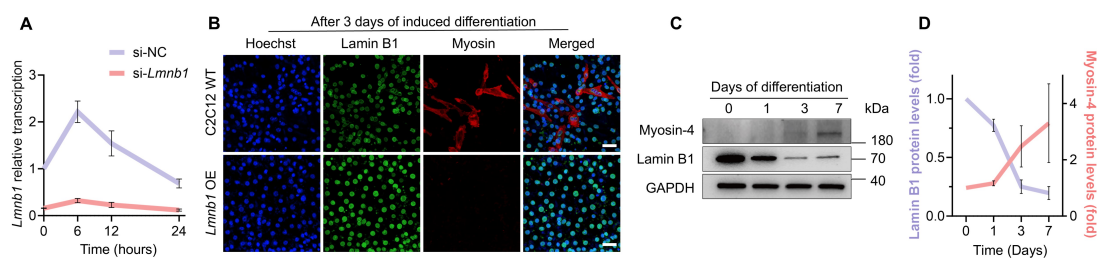


Figure EV5. Myoblast differentiation requires moderate lamin B1 protein levels.

(A) qPCR to examine the expression of *Lmnbl1* during 24 hours differentiation with scramble siRNA (si-NC) and si-*Lmnbl1*. $n = 3$. Data are presented as the mean \pm SD. (B) Representative images of WT and *Lmnbl1* overexpression C2C12 cells on petri-dishes with 2% horse serum induced differentiation for 3 days. scale bar, 50 μ m. (C, D) Western blot analysis of lamin B1 protein and Myosin-4 protein in C2C12 cells during 2% horse serum induced differentiation and corresponding intensity quantification data. $n = 3$. Data are presented as the mean \pm SD.